Fundamental Peregrine Solitons of Ultrastrong Amplitude Enhancement through Self-Steepening in Vector Nonlinear Systems

Shihua Chen,[1,*] Changchang Pan,[1] Philippe Grelu,[2] Fabio Baronio,[3,†] and Nail Akhmediev[4,‡]
[1]School of Physics, Southeast University, Nanjing 211189, China
[2]Laboratoire ICB, U.M.R. 6303 C.N.R.S., Université Bourgogne Franche-Comté, 9 avenue A. Savary, F-21078 Dijon, France
[3]INO CNR and Dipartimento di Ingegneria dell'Informazione, Università di Brescia, Via Branze 38, 25123 Brescia, Italy
[4]Department of Theoretical Physics, Research School of Physics, The Australian National University, Canberra ACT 2600, Australia

(Received 6 October 2019; accepted 2 March 2020; published 20 March 2020)

We report the universal emergence of anomalous fundamental Peregrine solitons, which can exhibit an unprecedentedly ultrahigh peak amplitude comparable to any higher-order rogue wave events, in the vector derivative nonlinear Schrödinger system involving the self-steepening effect. We present the exact explicit rational solutions on either a continuous-wave or a periodical-wave background, for a broad range of parameters. We numerically confirm the buildup of anomalous Peregrine solitons from strong initial harmonic perturbations, despite the onset of competing modulation instability. Our results may stimulate the experimental study of such Peregrine soliton anomaly in birefringent crystals or other similar vector systems.

DOI: 10.1103/PhysRevLett.124.113901

In the past decade, the field of rogue waves has rapidly grown and blossomed, involving researchers in various disciplines including oceanography, hydrodynamics, plasma physics, acoustics, optics and photonics, and even finance [1–4]. Among all the branches of rogue wave research, optical rogue waves, originally coined in a seminal paper by Solli *et al.* [5], are by far the most versatile and fast developing topic, thanks to the availability of reliable lasers, efficient materials, and real-time monitoring technologies [6,7]. In view of the unpredictability and complexity of rogue waves, the current investigations concentrate mainly on two different yet interlinked horizons: the study of the deterministic rogue wave events of integrable models [8–11] and of the emergent statistical properties of a large ensemble of incoherent waves [12–14]. Both ways enable a deep insight into the fundamental origin of rogue waves.

As a general building block for understanding rogue waves, the Peregrine soliton (PS), first proposed by Peregrine in 1983 [15], plays a central role in modeling the deterministic rogue wave events [16]. It is a doubly localized rational solution consisting of quadratic polynomials [10]. Normally, this solution involves a peak amplitude three times the background level [17–20] and an arbitrary peak location that agrees well with the fleeting nature of realistic rogue waves [21]. Considering its importance, several milestone experiments were conducted to observe this exotic structure or its variants [8,17,22,23]. Even in coupled nonlinear systems, typical PS structures exist as well, and are usually shown to have an enhancement factor smaller than 3 [24–28]. Recently, an anomaly of PS creation in a multicomponent system was reported, revealing explicitly that the PS structure can involve a peak amplitude beyond the factor 3 [29]. This is different from deterministic colliding events of ordinary solitons, which also entail an ultrahigh amplitude, yet predictable [30,31].

In this Letter, we would like to address an open yet interesting question: are the fundamental PSs involving an anomalous peak amplitude universal in physics? And if so, could their enhancement factor grow to an extent comparable to any higher-order rogue waves? To answer the first equation, one needs to consider the integrable models containing very few parameters so as to sieve out the effects of disturbing parameters. This will be met with the vector version of the derivative nonlinear Schrödinger (DNLS) equation [32], which involves only three basic ingredients: the group-velocity dispersion, Kerr nonlinearity, and self-steepening. With the help of this model and its general exact PS solutions built on a continuous-wave (cw) or a periodical-wave background, we find that the PS structures may possess a surprisingly ultralarge enhancement factor and that the self-steepening effect could play a crucial role in generating such a PS anomaly.

The vector DNLS equation, which governs the mixing of two fundamental-frequency (FF) pulses, denoted by u_1 and u_2, in a quadratic crystal via a type II highly phase-mismatched second-harmonic generation process, can be written as (in dimensionless form) [33–35]

$$i\frac{\partial u_1}{\partial \xi}+\frac{s}{2}\frac{\partial^2 u_1}{\partial \tau^2}+\left(1+i\epsilon\frac{\partial}{\partial \tau}\right)[(|u_1|^2+|u_2|^2)u_1]=0, \tag{1}$$

$$i\frac{\partial u_2}{\partial \xi}+\frac{s}{2}\frac{\partial^2 u_2}{\partial \tau^2}+\left(1+i\epsilon\frac{\partial}{\partial \tau}\right)[(|u_1|^2+|u_2|^2)u_2]=0, \quad (2)$$

where the cubic nonlinearity effect has also been taken into account. Here ξ is the normalized distance, and τ is the retarded time in a comoving frame at the envelope group velocity of the FF waves. The parameter s denotes the type of dispersion, i.e., $+1$ for anomalous dispersion and -1 for normal dispersion. The presence of the operator $[1+i\epsilon(\partial/\partial\tau)]$ in the nonlinear term gives rise to the self- and cross-phase modulation effects and the self-steepening effect denoted by the parameter ϵ, which becomes significant for pulses with spectral widths comparable to the optical frequency [33,36]. Basically, the parameter ϵ scales the perturbation to the Manakov system [37] and the latter is a popular model for optical pulses propagating in randomly birefringent fibers [38] or for crossing sea waves occurring in the open ocean [39]. It is known that this vector DNLS equation is integrable [40] and can therefore be solved by standard tools such as Darboux dressing technique.

PS solutions on a continuous background.—It is easy to show that Eqs. (1) and (2) have the plane-wave solutions

$$u_{j0}=a_j\exp(i\omega_j\tau-ik_j\xi), \qquad (j=1,2), \quad (3)$$

whose amplitudes (a_j), frequencies (ω_j), and wave numbers (k_j) are connected through the dispersion relations

$$k_j=\frac{1}{2}s\omega_j^2+(a_1^2+a_2^2)(\epsilon\omega_j-1). \quad (4)$$

Following the Darboux transformation procedure in Refs. [20,41], we obtain a general family of fundamental PS solutions on such a cw background:

$$u_1=u_{10}\left(1+\frac{R_1}{M-iN}\right)\left(\frac{M+iN}{M-iN}\right)\equiv U, \quad (5)$$

$$u_2=u_{20}\left(1+\frac{R_2}{M-iN}\right)\left(\frac{M+iN}{M-iN}\right)\equiv V, \quad (6)$$

where M, N, $R_{1,2}$ are polynomials of ξ and τ, given by

$$M=\theta^2+s^2\nu^2\xi^2+\frac{\eta^2}{4\alpha\nu^2}, \qquad N=\frac{\epsilon}{\alpha}(s\epsilon\nu^2\xi-\eta\theta), \quad (7)$$

$$R_j=\frac{2i[(\mu+\omega_j)\theta-s\nu^2\xi]}{(\mu+\omega_j)^2+\nu^2}-\frac{2\alpha+\eta(\epsilon\omega_j-1)}{\alpha[(\mu+\omega_j)^2+\nu^2]}, \quad (8)$$

with $\theta=\tau+[s\mu-\epsilon(a_1^2+a_2^2)]\xi$, $\eta=\epsilon\mu+1$, and $\alpha=\nu^2\epsilon^2+\eta^2$. The real parameters μ and ν in Eqs. (7) and (8) are determined by two algebraic equations:

$$s=\frac{[(\mu^2+\nu^2-\omega_1^2)(1-3\epsilon\omega_1)-4\epsilon\omega_1^2(\mu+\omega_1)]a_1^2}{[(\mu+\omega_1)^2+\nu^2]^2}+\frac{[(\mu^2+\nu^2-\omega_2^2)(1-3\epsilon\omega_2)-4\epsilon\omega_2^2(\mu+\omega_2)]a_2^2}{[(\mu+\omega_2)^2+\nu^2]^2}, \quad (9)$$

$$\frac{[\nu^2\epsilon+\eta(\mu+\omega_1)]a_1^2}{[(\mu+\omega_1)^2+\nu^2]^2}+\frac{[\nu^2\epsilon+\eta(\mu+\omega_2)]a_2^2}{[(\mu+\omega_2)^2+\nu^2]^2}=0. \quad (10)$$

We point out that the above rational PS solutions have been translated so that their peaks are located on the origin. Hence, one can readily define the peak-to-background ratios $\{[|u_1(0,0)|]/a_1\}$ and $\{[|u_2(0,0)|]/a_2\}$ as the enhancement factors $|f_{1,2}|$, respectively, with f_j being given by

$$f_j=1-\frac{8\nu^4\epsilon^2+4\nu^2(\epsilon\mu+1)(2\epsilon\mu+\epsilon\omega_j+1)}{(\epsilon\mu+1)^2[(\mu+\omega_j)^2+\nu^2]}. \quad (11)$$

These factors can be used to quantify the extent to which each PS component can be uplifted relative to its respective background. We would like to emphasize that the general solutions (5) and (6), as well as their enhancement factors obtained above, were not reported before, to our best knowledge. When $\epsilon=0$, our solutions can boil down to the PS solutions of the Manakov systems [24,25].

It follows easily from Eq. (11) that as $\epsilon=0$ (i.e., in the Manakov system limit), the enhancement factors of both PSs reduce to $|f_1^{\mathrm{Man}}|=|1-\{4\nu^2/[(\mu+\omega_1)^2+\nu^2]\}|\le 3$ and $|f_2^{\mathrm{Man}}|=|1-\{4\nu^2/[(\mu+\omega_2)^2+\nu^2]\}|\le 3$, which means that, when the self-steepening effect is absent, the peak amplitude of each PS component in either dispersion situation can never exceed the factor 3, as revealed before [9,24,25].

On the other hand, as $\delta=\omega_1-\omega_2=0$, we find from Eqs. (9) and (10) that $\mu=-\epsilon A/s-\omega_1$, $\nu=\sqrt{As(1-\epsilon\omega_1)-A^2\epsilon^2}/s$, where $A=a_1^2+a_2^2$. In this situation, it is easy to see that the solutions (5) and (6) become decoupled, each having a threefold peak amplitude, as found in the scalar Kaup-Newell equation [19,20].

In addition to the above two simple cases ($\epsilon=0$ or $\delta=0$), our fundamental PS solutions can exhibit an unprecedentedly high peak amplitude, in contrast to what is usually expected for the PS states. Over the years, such an ultralarge enhancement factor was attributed to the formation of higher-order rogue waves [20,42]. But now it is also achievable for the fundamental PS states, even though they involve only the second-degree polynomials.

To show this, let us first consider the special case for which the background amplitudes are specified by

$$a_1=\frac{4\sqrt{\delta^2 s(1-\epsilon\omega_1)^3}}{3\delta^2\epsilon^2+(\kappa\epsilon-2)^2}, \qquad a_2=\frac{4\sqrt{\delta^2 s(1-\epsilon\omega_2)^3}}{3\delta^2\epsilon^2+(\kappa\epsilon-2)^2}, \quad (12)$$

where $\delta = \omega_1 - \omega_2$ and $\kappa = \omega_1 + \omega_2$. Obviously, it requires that $s(1 - \epsilon\omega_j) > 0$, $(j = 1, 2)$, to make both amplitudes real. In this case, the algebraic Eqs. (9) and (10) will admit only one pair of real root (μ, ν):

$$\mu = \frac{\delta^2\epsilon(\kappa\epsilon - 8) - \kappa(\kappa\epsilon - 2)^2}{6\delta^2\epsilon^2 + 2(\kappa\epsilon - 2)^2}, \tag{13}$$

$$\nu = \frac{\sqrt{3}\delta[\delta^2\epsilon^2 - (\kappa\epsilon - 2)^2]}{6\delta^2\epsilon^2 + 2(\kappa\epsilon - 2)^2}. \tag{14}$$

Substituting the above μ and ν formulas into Eq. (11) reveals that the maximum enhancement factor can reach as high as 17, much larger than that shown in Ref. [29]. Typical results are shown in Fig. 1, where an eightfold peak amplitude in the u_1 component is exhibited, in either the anomalous [Figs. 1(a) and 1(b)] or normal dispersion [Figs. 1(c) and 1(d)] situation. This represents an anomaly of the PS formation, as, when ϵ vanishes, the peak amplitude is only twice the background height, as shown in Figs. 1(e) and 1(f). Clearly, in such an unusual PS dynamics, the unique role of the self-steepening effect can be highlighted, which induces a dip in the structure of the strong component, while making Peregrine rogue wave soar on the weak component.

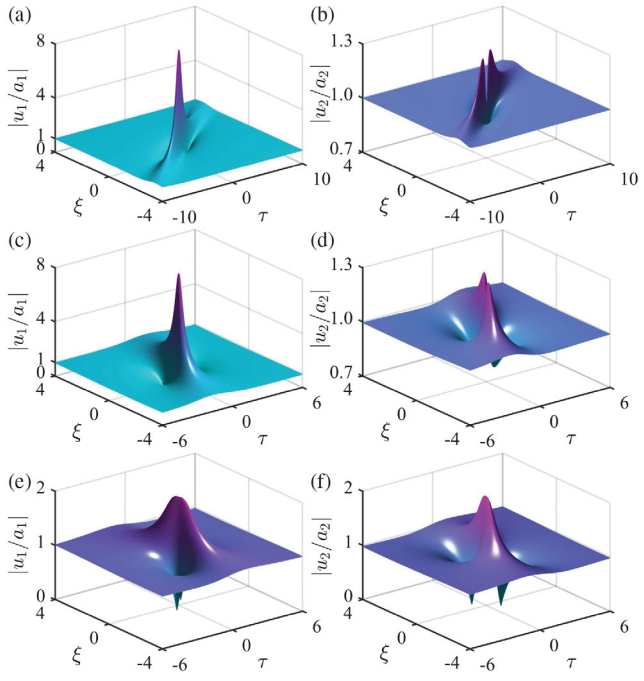

FIG. 1. Unusual fundamental PSs in the (a),(b) anomalous dispersion ($s = 1$) and (c),(d) normal dispersion ($s = -1$) regimes, normalized to their respective backgrounds (letting $\epsilon = 1$). The other parameters are given by (a),(b) $\omega_1 = -1/4$, $\omega_2 = -11/4$, $a_1 = \sqrt{5}/7$, $a_2 = 3\sqrt{15}/7$; (c),(d) $\omega_1 = 2$, $\omega_2 = 4$, $a_1 = 2/7$, $a_2 = 6\sqrt{3}/7$. The specific PS states in the Manakov system ($\epsilon = 0$) are plotted in (e) and (f), with $s = 1$, $\omega_1 = 1/2$, $\omega_2 = -1/2$, $a_1 = a_2 = 1$.

We show further that our PS solutions can allow two different PS structures for each component under conditions other than Eq. (12), and one PS structure would have a very large amplitude factor, even approaching infinity. As an example, let us consider the amplitude condition:

$$a_1 = \sqrt{\frac{s(1 - \epsilon\omega_1)^3}{\epsilon^2(\kappa\epsilon - 2)^2}}, \qquad a_2 = \sqrt{\frac{s(1 - \epsilon\omega_2)^3}{\epsilon^2(\kappa\epsilon - 2)^2}}, \tag{15}$$

where $s(1 - \epsilon\omega_{1,2}) > 0$, the same as in Eq. (12). Then, it is easy to solve the algebraic Eqs. (9) and (10) for (μ, ν). One can find that under the specific condition (15), there will exist two pairs of valid values of (μ, ν), and hence two enhancement factors for each PS component, as shown in Fig. 2, where we present the evolutions of f_1 and f_2 with respect to δ, for given parameters $\epsilon = 1$, $s = -1$, and $\kappa = 6$. As seen, when $\delta = -2$, the u_1 component has an enhancement factor $|f_1| = 11.0$ (blue cross) and 3.51 (red circle), while the u_2 component has a factor $|f_2| = 1.66$ (blue cross) and 1.11 (red circle), respectively. The corresponding PS structures are demonstrated in the insets in Fig. 2. Apparently, these two PS structures can coexist on the same continuous background, as revealed in Ref. [26]. Moreover, it suggests that as $\delta \to \pm(2/\epsilon - \kappa)$ (here $\delta \to \mp 4$), the enhancement factor of the u_1 or u_2 component can approach infinity, although in this case its background amplitude a_1 or a_2 will approach zero too, as indicated by the green dashed line in Fig. 2.

PS solutions on a periodical background.—Furthermore, the rational solutions that represent the PS states built on a periodical-wave background [43,44] can be given by

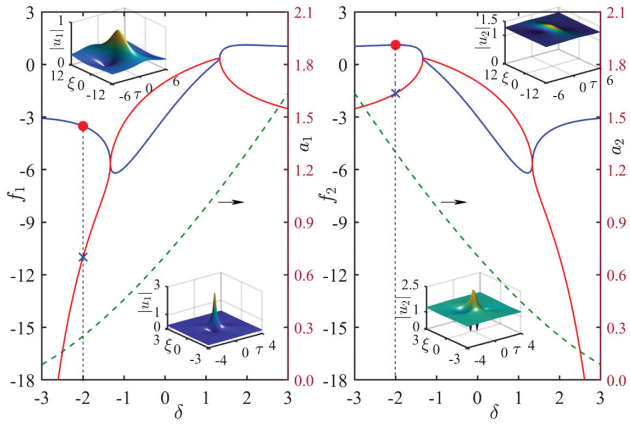

FIG. 2. Evolutions of f_1 and f_2 versus $\delta = \omega_1 - \omega_2$ for $\epsilon = 1$, $s = -1$, and $\kappa = 6$. The green dashed line gives the values of a_1 and a_2 specified by Eq. (15), which can be read from the vertical axis that the black arrow points to. In each panel, the insets show the PS structures at $\delta = -2$, with the upper and lower plots corresponding to the red solid circle and blue cross, respectively.

$$u_1 = \frac{\sqrt{2}}{2}(U+V), \qquad u_2 = \frac{\sqrt{2}}{2}(U-V), \tag{16}$$

where U and V are defined by Eqs. (5) and (6), with all the parameters kept the same. As a typical example, we demonstrate in Fig. 3 two pairs of PS solutions that coexist on the same periodical wave background, in the normal dispersion regime. For direct comparison, we exploited the same parameters as used in the insets in Fig. 2. This set of background parameters gives two pairs of valid values (μ,ν) (see caption), each yielding a PS structure on a periodical wave background. It is seen that in Figs. 3(a) and 3(b), the PS solutions have a larger transversal size and tend to interfere with the periodical waves, while maintaining a PS profile as a whole. However, in Figs. 3(c) and 3(d), the PS solutions are smaller in size and thus can manifest predominantly on the periodical background. In the latter situation, the peak-to-background factor is around 3.5, lower than the factor 11 as indicated in Fig. 2, but still higher than 3.

To see the mechanism behind this PS anomaly, one may evaluate the modulation instability (MI) by perturbing the background fields (3) as $u_j = u_{j0}\{1 + p_j \exp[-i\Omega(\beta\xi - \tau)] + q_j^* \exp[i\Omega(\beta^*\xi - \tau)]\}$ $(j = 1, 2)$, where p_j and q_j are small parameters, and Ω and β are positive and complex, respectively [1,10]. Then, substitution of these perturbed solutions into Eqs. (1) and (2) followed by linearization yields a quartic equation of β, from which the gain $\gamma_h = \Omega|\mathrm{Im}(\beta)|$ in any dispersion cases can be calculated. Figures 4(a) and 4(b) show the gain map γ_h versus Ω and δ for the DNLS and Manakov systems, respectively, in the normal dispersion case. It is exhibited that in the Manakov system, the baseband gain spectra located symmetrically in a limited range of δ as $\Omega \to 0$ [25], whereas in the DNLS system, they may exist in a broad δ region, asymmetrically yet more strongly (see the white dashed line). The latter can lead to the anomalous PS behaviors in a broad range of parameters, according to the baseband MI theory [10,25,45]. For instance, for the specific parameters used in Figs. 1(c) and 1(d), the gain maximum is $\gamma_h^{\max} \approx 1.30$ occurring at $\Omega \approx 1.87$. This small gain value suggests that an eightfold PS structure could be reproduced numerically.

Finally, to confirm our analytical predictions, we performed extensive numerical simulations of Eqs. (1) and (2), using the split-step Fourier method [29,45], where the nonlinear step is treated in the time domain, while the linear step is evaluated pseudospectrally. Typical simulation results are shown in Fig. 5, where we use the same system parameters as in Figs. 1(c) and 1(d). We first show in Figs. 5(a) and 5(b) that, evolving from the initial analytical profiles at $\xi = -3$, an eightfold-amplitude PS for the u_1 field and a much gentler structure for the u_2 field are exactly reproduced. Then, we put small-amplitude harmonic waves on these initial profiles at $\xi = -1$ and find that the whole PS structures still emerge [see Figs. 5(c) and 5(d)]. In this situation, due to the competing MI process, some even higher-amplitude Peregrine rogue waves, with a factor of nearly 12, manifest as well (at around $\xi = 2$). This is not surprising because the amplitude condition Eq. (12) that we exploited here will be violated to an extent under strong initial perturbations, resulting in the appearance of coexisting rogue waves that may have an even higher enhancement factor, as suggested in Fig. 2. Lastly, we confirm numerically that PS solutions of unprecedentedly large factor can be excited from a turbulent wave field. To do so, we use the plane-wave solutions (3) at $\xi = -1$ as initial conditions, perturbed by five harmonic waves of random strength. This noisy background subsequently develops into a turbulent sea of different waves, among

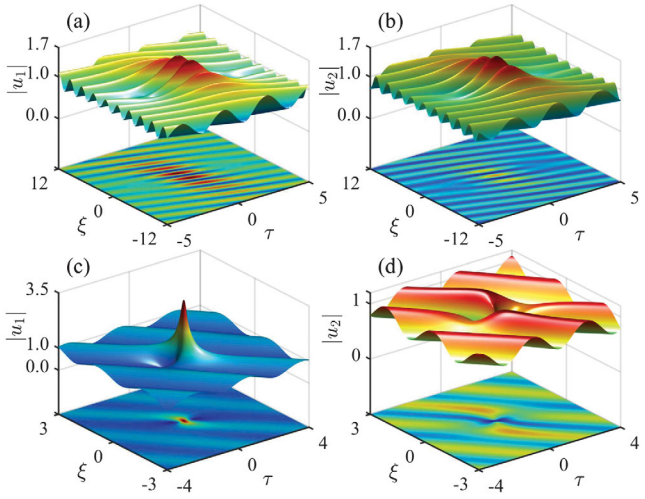

FIG. 3. Surface (top) and contour (bottom) plots of fundamental PS solutions on the same periodical wave background, with parameters $\epsilon = 1$, $s = -1$, $\omega_1 = 2$, $\omega_2 = 4$, $a_1 = 1/4$, and $a_2 = 3\sqrt{3}/4$. (a),(b) $(\mu,\nu) = (-17/8 + \sqrt{3}/8, 3\sqrt{5}/8 - \sqrt{15}/8)$; (c), (d) $(\mu,\nu) = (-17/8 - \sqrt{3}/8, 3\sqrt{5}/8 + \sqrt{15}/8)$.

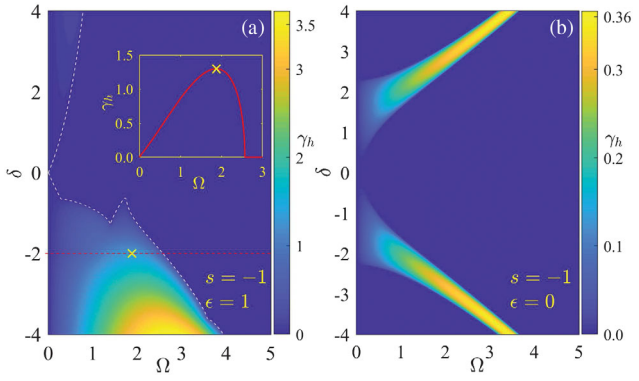

FIG. 4. Maps of MI gain γ_h versus Ω and δ for the (a) DNLS and (b) Manakov systems, under otherwise identical parameter condition, i.e., $\kappa = 6$, $a_1 = 2/7$, and $a_2 = 6\sqrt{3}/7$. The inset in (a) shows the gain profile γ_h at $\delta = -2$, and the yellow cross indicates the maximum gain $\gamma_h^{\max} \approx 1.30$ at $\Omega \approx 1.87$.

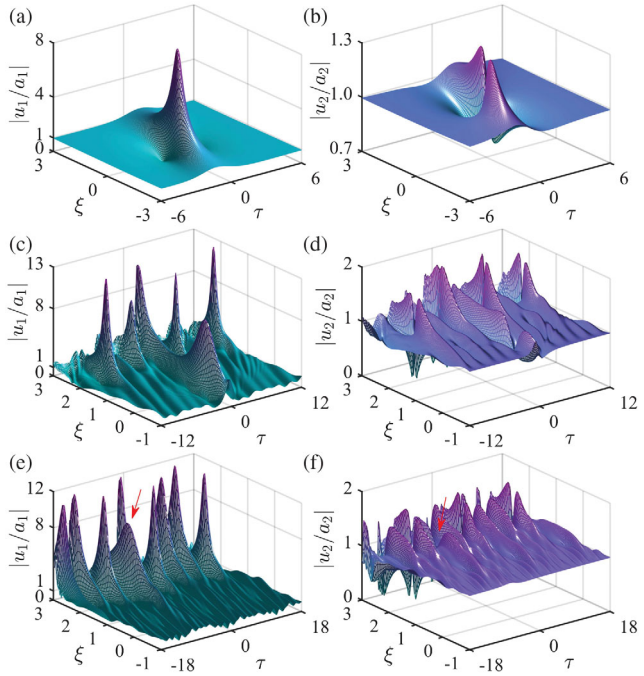

FIG. 5. Numerical recurrence of an eightfold-amplitude PS shown in Figs. 1(c) and 1(d) from (a),(b) the analytical solutions (5) and (6) at $\xi = -3$; (c),(d) the initial profiles at $\xi = -1$ but perturbed by low-amplitude harmonic waves; and (e),(f) the plane-wave solutions (3) at $\xi = -1$ perturbed by low-amplitude harmonic waves, respectively, under otherwise identical conditions.

which one eightfold PS structure, at around $(\xi, \tau) = (2, -5)$, could be singled out, see the red arrow in Figs. 5(e) and 5(f). It is hence anticipated that these deterministic PS structures might be observed in a laboratorial environment [46].

In summary, we have drawn several significant points here. First, to achieve the ultrahigh PS structures, a multicomponent nonlinear coupling is indispensable, as it enables the energy transfer between different components so that one component can grow at the expense of the other [47]. Second, the PS structure of ultrahigh factor always forms on a weaker background. We may argue that the stronger background field serves as an energy reservoir to pump the weaker one via a two-wave coupling [48], producing, in realistic noisy conditions, a turbulent wave field that gives birth to the anomalous PS structures. Last, being at the origin of the PS anomaly, the role of the self-steepening effect can not be overemphasized [29]. As the self-steepening effect is inherent in many systems (e.g., quadratic nonlinear media [33,34], optical fibers and waveguides [38,49,50], and alkali vapors [51]), this also suggests the universality of our PS solutions to be observed in diverse settings. For example, we may launch two FF pulses of picosecond duration, which can mimic quasi-cw signals, in a twin $KTiOPO_4$ crystal device to trigger a temporal type-II (*oeo*) second-harmonic generation with a low walk-off angle [52]. In this case, the two-wave anomalous PS dynamics may be seen in the highly phase-mismatched regime.

This work was supported by the National Natural Science Foundation of China (Grants No. 11474051 and No. 11974075) and by the European Union under the European Unions Horizon 2020 research and innovation program MSCA-RISE-2015 (Grant No. 691051). Ph. G. acknowledges support from the Engineering and Innovation through Physical Sciences, High-technologies, and Cross-disciplinary research (EIPHI) Graduate School (Contract No. ANR-17-EURE-0002). The authors also thank John M. Dudley and Stefan Wabnitz for stimulating discussions regarding the fundamental model.

*cshua@seu.edu.cn
†fabio.baronio@unibs.it
‡nail.akhmediev@anu.edu.au

[1] J. M. Dudley, F. Dias, M. Erkintalo, and G. Genty, Instabilities, breathers and rogue waves in optics, Nat. Photonics **8**, 755 (2014).
[2] M. Onorato, S. Residori, U. Bortolozzo, A. Montina, and F. T. Arecchi, Rogue waves and their generating mechanisms in different physical contexts, Phys. Rep. **528**, 47 (2013).
[3] Y.-Y. Tsai, J.-Y. Tsai, and L. I, Generation of acoustic rogue waves in dusty plasmas through three-dimensional particle focusing by distorted waveforms, Nat. Phys. **12**, 573 (2016).
[4] *Nonlinear Guided Wave Optics: A testbed for extreme waves*, edited by S. Wabnitz (IOP Publishing, Bristol, 2017).
[5] D. R. Solli, C. Ropers, P. Koonath, and B. Jalali, Optical rogue waves, Nature (London) **450**, 1054 (2007).
[6] M. Närhi, B. Wetzel, C. Billet, S. Toenger, T. Sylvestre, J.-M. Merolla, R. Morandotti, F. Dias, G. Genty, and J. M. Dudley, Real-time measurements of spontaneous breathers and rogue wave events in optical fibre modulation instability, Nat. Commun. **7**, 13675 (2016).
[7] A. Tikan, S. Bielawski, C. Szwaj, S. Randoux, and P. Suret, Single-shot measurement of phase and amplitude by using a heterodyne time-lens system and ultrafast digital time-holography, Nat. Photonics **12**, 228 (2018).
[8] B. Kibler, J. Fatome, C. Finot, G. Millot, F. Dias, G. Genty, N. Akhmediev, and J. M. Dudley, The Peregrine soliton in nonlinear fibre optics, Nat. Phys. **6**, 790 (2010).
[9] F. Baronio, A. Degasperis, M. Conforti, and S. Wabnitz, Solutions of the Vector Nonlinear Schrödinger Equations: Evidence for Deterministic Rogue Waves, Phys. Rev. Lett. **109**, 044102 (2012).
[10] S. Chen, F. Baronio, J. M. Soto-Crespo, Ph. Grelu, and D. Mihalache, Versatile rogue waves in scalar, vector, and multidimensional nonlinear systems, J. Phys. A **50**, 463001 (2017).
[11] A. Tikan, C. Billet, G. El, A. Tovbis, M. Bertola, T. Sylvestre, F. Gustave, S. Randoux, G. Genty, P. Suret, and J. M. Dudley, Universality of the Peregrine Soliton in the Focusing Dynamics of the Cubic Nonlinear Schrödinger Equation, Phys. Rev. Lett. **119**, 033901 (2017).

[12] C. Lecaplain, P. Grelu, J. M. Soto-Crespo, and N. Akhmediev, Dissipative Rogue Waves Generated by Chaotic Pulse Bunching in a Mode-Locked Laser, Phys. Rev. Lett. **108**, 233901 (2012).
[13] D. Pierangeli, F. Di Mei, C. Conti, A. J. Agranat, and E. DelRe, Spatial Rogue Waves in Photorefractive Ferroelectrics, Phys. Rev. Lett. **115**, 093901 (2015).
[14] J. M. Soto-Crespo, N. Devine, and N. Akhmediev, Integrable Turbulence and Rogue Waves: Breathers or Solitons?, Phys. Rev. Lett. **116**, 103901 (2016).
[15] D. H. Peregrine, Water waves, nonlinear Schrödinger equations and their solutions, J. Aust. Math. Soc. Series B, Appl. Math. **25**, 16 (1983).
[16] V. I. Shrira and V. V. Geogjaev, What makes the Peregrine soliton so special as a prototype of freak waves?, J. Eng. Math. **67**, 11 (2010).
[17] A. Chabchoub, N. P. Hoffmann, and N. Akhmediev, Rogue Wave Observation in a Water Wave Tank, Phys. Rev. Lett. **106**, 204502 (2011).
[18] H. N. Chan, K. W. Chow, D. J. Kedziora, R. H. J. Grimshaw, and E. Ding, Rogue wave modes for a derivative nonlinear Schrödinger model, Phys. Rev. E **89**, 032914 (2014).
[19] S. Chen, F. Baronio, J. M. Soto-Crespo, Y. Liu, and P. Grelu, Chirped Peregrine solitons in a class of cubic-quintic nonlinear Schrödinger equations, Phys. Rev. E **93**, 062202 (2016).
[20] S. Chen, Y. Zhou, L. Bu, F. Baronio, J. M. Soto-Crespo, and D. Mihalache, Super chirped rogue waves in optical fibers, Opt. Express **27**, 11370 (2019).
[21] N. Akhmediev, A. Ankiewicz, and M. Taki, Waves that appear from nowhere and disappear without a trace, Phys. Lett. A **373**, 675 (2009).
[22] H. Bailung, S. K. Sharma, and Y. Nakamura, Observation of Peregrine Solitons in a Multicomponent Plasma with Negative Ions, Phys. Rev. Lett. **107**, 255005 (2011).
[23] B. Frisquet, B. Kibler, Ph. Morin, F. Baronio, M. Conforti, G. Millot, and S. Wabnitz, Optical dark rogue wave, Sci. Rep. **6**, 20785 (2016).
[24] S. Chen and D. Mihalache, Vector rogue waves in the Manakov system: Diversity and compossibility, J. Phys. A **48**, 215202 (2015).
[25] F. Baronio, M. Conforti, A. Degasperis, S. Lombardo, M. Onorato, and S. Wabnitz, Vector Rogue Waves and Baseband Modulation Instability in the Defocusing Regime, Phys. Rev. Lett. **113**, 034101 (2014).
[26] S. Chen, J. M. Soto-Crespo, and Ph. Grelu, Coexisting rogue waves within the $(2+1)$-component long-wave–short-wave resonance, Phys. Rev. E **90**, 033203 (2014).
[27] F. Baronio, M. Conforti, A. Degasperis, and S. Lombardo, Rogue Waves Emerging from the Resonant Interaction of Three Waves, Phys. Rev. Lett. **111**, 114101 (2013).
[28] S. Chen, Y. Ye, F. Baronio, Y. Liu, X.-M. Cai, and P. Grelu, Optical Peregrine rogue waves of self-induced transparency in a resonant erbium-doped fiber, Opt. Express **25**, 29687 (2017).
[29] S. Chen, Y. Ye, J. M. Soto-Crespo, P. Grelu, and F. Baronio, Peregrine Solitons Beyond the Threefold Limit and Their Two-Soliton Interactions, Phys. Rev. Lett. **121**, 104101 (2018).
[30] A. V. Slunyaev and E. N. Pelinovsky, Role of Multiple Soliton Interactions in the Generation of Rogue Waves: The Modified Korteweg–de Vries Framework, Phys. Rev. Lett. **117**, 214501 (2016).
[31] S. Chen, Y. Zhou, F. Baronio, and D. Mihalache, Special types of elastic resonant soliton solutions of the Kadomtsev–Petviashvili II equation, Rom. Rep. Phys. **70**, 102 (2018).
[32] V. A. Vysloukh and I. V. Cherednik, Many-soliton components of solutions of nonlinear Schrödinger equation with perturbing term, Theor. Math. Phys. **78**, 24 (1989).
[33] J. Moses and F. W. Wise, Controllable Self-Steepening of Ultrashort Pulses in Quadratic Nonlinear Media, Phys. Rev. Lett. **97**, 073903 (2006).
[34] J. Moses, B. A. Malomed, and F. W. Wise, Self-steepening of ultrashort optical pulses without self-phase-modulation, Phys. Rev. A **76**, 021802(R) (2007).
[35] M. Conforti, F. Baronio, and S. Trillo, Dispersive shock waves in phase-mismatched second-harmonic generation, Opt. Lett. **37**, 1082 (2012).
[36] A. L. Gaeta, Catastrophic Collapse of Ultrashort Pulses, Phys. Rev. Lett. **84**, 3582 (2000).
[37] J. U. Kang, G. I. Stegeman, J. S. Aitchison, and N. Akhmediev, Observation of Manakov Spatial Solitons in AlGaAs Planar Waveguides, Phys. Rev. Lett. **76**, 3699 (1996).
[38] G. P. Agrawal, *Nonlinear Fiber Optics*, 4th ed. (Academic, San Diego, 2007).
[39] M. Onorato, A. R. Osborne, and M. Serio, Modulational Instability in Crossing Sea States: A Possible Mechanism for the Formation of Freak Waves, Phys. Rev. Lett. **96**, 014503 (2006).
[40] M. Hisakado and M. Wadati, Integrable Multi-Component Hybrid Nonlinear Schrödinger Equations, J. Phys. Soc. Jpn. **64**, 408 (1995).
[41] Y. Ye, Y. Zhou, S. Chen, F. Baronio, and P. Grelu, General rogue wave solutions of the coupled Fokas–Lenells equations and non-recursive Darboux transformation, Proc. R. Soc. A **475**, 20180806 (2019).
[42] A. Chabchoub, N. Hoffmann, M. Onorato, and N. Akhmediev, Super Rogue Waves: Observation of a Higher-Order Breather in Water Waves, Phys. Rev. X **2**, 011015 (2012).
[43] W. Liu, Y. Zhang, and J. He, Rogue wave on a periodic background for Kaup–Newell equation, Rom. Rep. Phys. **70**, 106 (2018).
[44] L.-C. Zhao, L. Duan, P. Gao, and Z.-Y. Yang, Vector rogue waves on a double-plane wave background, Europhys. Lett. **125**, 40003 (2019).
[45] F. Baronio, S. Chen, Ph. Grelu, S. Wabnitz, and M. Conforti, Baseband modulation instability as the origin of rogue waves, Phys. Rev. A **91**, 033804 (2015).
[46] F. Baronio, B. Frisquet, S. Chen, G. Millot, S. Wabnitz, and B. Kibler, Observation of a group of dark rogue waves in a telecommunication optical fiber, Phys. Rev. A **97**, 013852 (2018).
[47] N. S. Ginzburg, R. M. Rozental, A. S. Sergeev, A. E. Fedotov, I. V. Zotova, and V. P. Tarakanov, Generation of

Rogue Waves in Gyrotrons Operating in the Regime of Developed Turbulence, Phys. Rev. Lett. **119**, 034801 (2017).

[48] R. W. Boyd, *Nonlinear Optics*, 3rd ed. (San Diego, Academic, 2008).

[49] B. Wetzel, D. Bongiovanni, M. Kues, Y. Hu, Z. Chen, S. Trillo, J. M. Dudley, S. Wabnitz, and R. Morandotti, Experimental Generation of Riemann Waves in Optics: A Route to Shock Wave Control, Phys. Rev. Lett. **117**, 073902 (2016).

[50] D. Anderson and M. Lisak, Nonlinear asymmetric self-phase modulation and self-steepening of pulses in long optical waveguides, Phys. Rev. A **27**, 1393 (1983).

[51] D. Grischkowsky, E. Courtens, and J. A. Armstrong, Observation of Self-Steepening of Optical Pulses with Possible Shock Formation, Phys. Rev. Lett. **31**, 422 (1973).

[52] J.-J. Zondy, M. Abed, and S. Khodja, Twin-crystal walk-off-compensated type-II second-harmonic generation: Single-pass and cavity-enhanced experiments in $KTiOPO_4$, J. Opt. Soc. Am. B **11**, 2368 (1994).